Geophysical Research Letters

RESEARCH LETTER
10.1029/2023GL103419

Monitoring Terrestrial Water Storage, Drought and Seasonal Changes in Central Oklahoma With Ambient Seismic Noise

Shuo Zhang[1], Bingxu Luo[1], Yehuda Ben-Zion[2], David E. Lumley[1,3], and Hejun Zhu[1,3]

[1]Department of Geosciences, The University of Texas at Dallas, Richardson, TX, USA, [2]Department of Earth Science and Southern California Earthquake Center, University of Southern California, Los Angeles, CA, USA, [3]Department of Physics, The University of Texas at Dallas, Richardson, TX, USA

Key Points:

- A long-term trend of *dv/v* in Oklahoma correlates well with gravity measurements, which may reflect groundwater recharge and discharge
- Short-term peaks of *dv/v* agree with the drought index, demonstrating a potential for monitoring meteorological droughts
- A seasonal cycle of *dv/v* in central Oklahoma can be explained by thermo-elastic strains driven by atmospheric temperature changes

Supporting Information:

Supporting Information may be found in the online version of this article.

Correspondence to:

H. Zhu,
hejun.zhu@utdallas.edu

Citation:

Zhang, S., Luo, B., Ben-Zion, Y., Lumley, D. E., & Zhu, H. (2023). Monitoring terrestrial water storage, drought and seasonal changes in central Oklahoma with ambient seismic noise. *Geophysical Research Letters*, *50*, e2023GL103419. https://doi.org/10.1029/2023GL103419

Received 23 FEB 2023
Accepted 13 AUG 2023

Author Contributions:

Conceptualization: Hejun Zhu
Data curation: Shuo Zhang
Formal analysis: Shuo Zhang, Hejun Zhu
Funding acquisition: Hejun Zhu
Investigation: Shuo Zhang, Hejun Zhu
Methodology: Shuo Zhang, Bingxu Luo, Yehuda Ben-Zion, Hejun Zhu
Project Administration: Hejun Zhu
Resources: David E. Lumley, Hejun Zhu
Supervision: Yehuda Ben-Zion, David E. Lumley, Hejun Zhu
Validation: Shuo Zhang, Bingxu Luo
Visualization: Shuo Zhang
Writing – original draft: Shuo Zhang

Abstract Significant imbalances in terrestrial water storage (TWS) and severe drought have been observed around the world as a consequence of climate changes. Improving our ability to monitor TWS and drought is critical for water-resource management and water-deficit estimation. We use continuous seismic ambient noise to monitor temporal evolution of near-surface seismic velocity, *dv/v*, in central Oklahoma from 2013 to 2022. The derived *dv/v* is found to be negatively correlated with gravitational measurements and groundwater depths, showing the impact of groundwater storage on seismic velocities. The hydrological effects involving droughts and recharge of groundwater occur on a multi-year time scale and dominate the overall derived velocity changes. The thermoelastic response to atmospheric temperature variations occurs primarily on a yearly timescale and dominates the superposed seasonal velocity changes in this study. The occurrences of droughts appear simultaneously with local peaks of *dv/v*, demonstrating the sensitivity of near-surface seismic velocities to droughts.

Plain Language Summary Terrestrial water storage (TWS) is fundamental to the well-being of inhabitants on Earth. However, current approaches to measure TWS variations have limited temporal or spatial resolution. In this study, we use near-surface seismic velocity variations, *dv/v*, derived from continuous seismic recordings to monitor changes of TWS in central Oklahoma. A negative correlation between the long-term trend of *dv/v* with gravity measurements reflects the impact of groundwater recharge/discharge on near-surface seismic velocity. In addition, a seasonal cycling of *dv/v* has similar periodicity to recordings of air temperature, which can be explained by thermo-elastic strain at the subsurface. Comparisons between *dv/v* and drought index further show the possibility of using near-surface seismic velocity as a proxy for monitoring severe drought for local communities. Considering the high temporal sampling and flexible spatial deployment, seismometers may be used to monitor subsurface water distributions. This can be useful for sustainable water management and reliable water-deficit estimation.

1. Introduction

Terrestrial water storage (TWS), which mainly includes groundwater, surface water, soil moisture, snow and ice accumulation plays important roles in many studies including the Earth's hydrological cycle (Famiglietti et al., 2011; Oki & Kanae, 2006), climate change (Pokhrel et al., 2021; Rodell et al., 2018), sea-level (Konikow, 2011; J. Reager et al., 2016), drought (Rodell et al., 2009) and flooding (J. T. Reager et al., 2014). The groundwater and surface water are dominant prerequisites for agricultural irrigation, and have important social- and economical-impact to modern society (Famiglietti et al., 2011; Rodell et al., 2009; Scanlon et al., 2012). Severe climate changes have also led to frequent occurrences of drought and flooding. In addition, increasing demands on water resources for economical and social developments have imposed tremendous stresses on TWS (Feng et al., 2013; Long et al., 2013). Hence, it is critical to accurately and timely monitor the change of TWS in order to maintain sustainable water-resources management and rational water-inadequacy estimation (Alsdorf & Lettenmaier, 2003).

Direct measurements of TWS, such as installing gauges in wells, can accurately assess the levels of aquifers. However, due to the expense of well drilling and instrument maintenance, a limited number of wells typically lead to TWS estimates with a low spatial resolution (Alsdorf & Lettenmaier, 2003). In contrast, remote sensing techniques, such as Global Positioning System (GPS) and Interferometric Synthetic Aperture Radar (InSAR), allow measuring the deformation of the Earth's surface, which can then be used to infer groundwater variations

Writing – review & editing: Yehuda Ben-Zion, David E. Lumley, Hejun Zhu

and underground fluid migration (Argus et al., 2005; Bawden et al., 2001). In spite of the high temporal resolution of GPS measurements (K. H. Ji & Herring, 2012), its point-sampling characteristics fail to accurately map lateral heterogeneity of TWS. On the other hand, radar and InSAR can be used to delineate surface deformation with a much higher spatial resolution (Lanari et al., 2004; Watson et al., 2002), but they typically suffer from comparatively low temporal resolution, which depends on the orbital frequency of satellites. Since 2003, the Gravity Recovery and Climate Experiment (GRACE), a joint mission supported by the National Aeronautics and Space Administration (NASA) and the German Aerospace Center, provides detailed information on gravity variations on the Earth's surface by measuring the position changes of twin satellites (Tapley, Bettadpur, Watkins, & Reigber, 2004), which can be related to changes in gravitational acceleration and mass distribution. These temporal mass changes near the Earth's surface primarily result from near-surface water circulation and migration. As a state-of-the-art technique, GRACE measurements have been widely used to assess TWS variations from regional to global scales (Rodell et al., 2007; Tian et al., 2017), and also enable estimating ice sheet and glacier melting in Greenland and Antarctica (Harig & Simons, 2012; Velicogna & Wahr, 2006a, 2006b). However, its limited temporal sampling (one month) and spatial resolution (around 300–400 km) (Tapley, Bettadpur, Watkins, & Reigber, 2004) cannot satisfy the urgent requirement of managing sustainable water-resource at regional to local scales.

There have been many applications for time-lapse seismic velocity analysis of water injection (Landrø, 2001; Nakata et al., 2022), reservoir monitoring (Angerer et al., 2002; Rickett & Lumley, 2001), and carbon capture and storage (D. Lumley, 2010; Zhu et al., 2019). Because of data availability and computational cost, these classical approaches to monitor temporal changes of the seismic velocities is limited by the occurrence of earthquakes in small regions, which commonly leads to sparse temporal sampling (D. E. Lumley, 2001; Kamei & Lumley, 2017). Over the past decades, continuously recorded seismic ambient noise has been widely used to delineate spatial and temporal variations of seismic velocities within the Earth's crust and upper mantle. This alleviates the restriction of using ballistic wave propagation between earthquakes and seismometers (Campillo & Paul, 2003; Lin et al., 2008; Ritzwoller et al., 2011; Shapiro et al., 2005; Yao & Van Der Hilst, 2009), thus enabling the imaging of Earth's structure for seismically inactive regions. A diffusive wavefield generated by noise source that persistent in time can be used to extract the Green's function from continuous seismic recordings and analyze temporal changes of seismic velocities (Claerbout, 1968; Lobkis & Weaver, 2001; Sens-Schönfelder & Wegler, 2006; Snieder, 2006; Wapenaar & Fokkema, 2006). As examples, co- and post-seismic damage and healing processes were studied by measuring seismic velocity changes before and after large earthquakes in California (Brenguier, Campillo, et al., 2008; Lu & Ben-Zion, 2022; Taira et al., 2015), Sichuan (Liu et al., 2014; Pei et al., 2019), Tohoku area (Brenguier et al., 2014; Minato et al., 2012; Rubinstein et al., 2007), and Turkey (Peng & Ben-Zion, 2006). Some studies also demonstrated the potential of using seismic ambient noise to study environmental changes, such as investigating correlations between near-surface seismic velocity changes with precipitation (H. F. Wang, 2017; Q. Wang et al., 2017), temperature changes (Hillers & Ben-Zion, 2011; Wu et al., 2020), freeze-thaw of permafrost (James et al., 2017; Lindner et al., 2021), periodic ocean tide (Ardhuin et al., 2011; Mao et al., 2019; Sens-Schönfelder & Eulenfeld, 2019; Takano et al., 2019), and CO_2 injection (Gassenmeier et al., 2014). Several studies utilized ambient noise recordings to monitor crustal velocity changes in response to severe droughts in California (Clements & Denolle, 2018; Mao et al., 2022) and Texas (Kim & Lekic, 2019), moisture condition in Southern Himalayan (Illien et al., 2021), as well as decadal hydrological and temperature changes in southern Germany (Lecocq et al., 2017).

Following previous studies, we aim to use continuous seismic recordings to monitor TWS and drought in Oklahoma. As an agricultural state, irrigation in Oklahoma highly depends on the supply of groundwater. Detected by the U.S. Drought Monitor (Svoboda et al., 2002), central Oklahoma has suffered from severe droughts in the last decade (Kuwayama et al., 2019). The U.S. is the world's third-largest wheat exporter, and severe droughts in these two major wheat-producing states, Kansas and Oklahoma, led to 7%–8% reduction of wheat in 2021 in comparison to their 5-year average (Stephanie Hegarty, 2022). Improving the capability to better monitor water storage in Oklahoma can contribute to sustainable water resources management and steady global food supplies. Deployed by the United States Geological Survey and Oklahoma Geological Survey (OGS), the large amounts of permanent and temporary seismometers in Oklahoma provide an important opportunity to investigate environmental changes via seismic ambient noise, and in particular to monitor variations of TWS and droughts in central Oklahoma. Two major bedrock aquifers in central Oklahoma are the Garber-Wellington (GW) in the south and the Vamoosa-Ada in the east (Figure 1a). Several minor reservoirs, such as the Enid Isolated Terrace, Cimarron

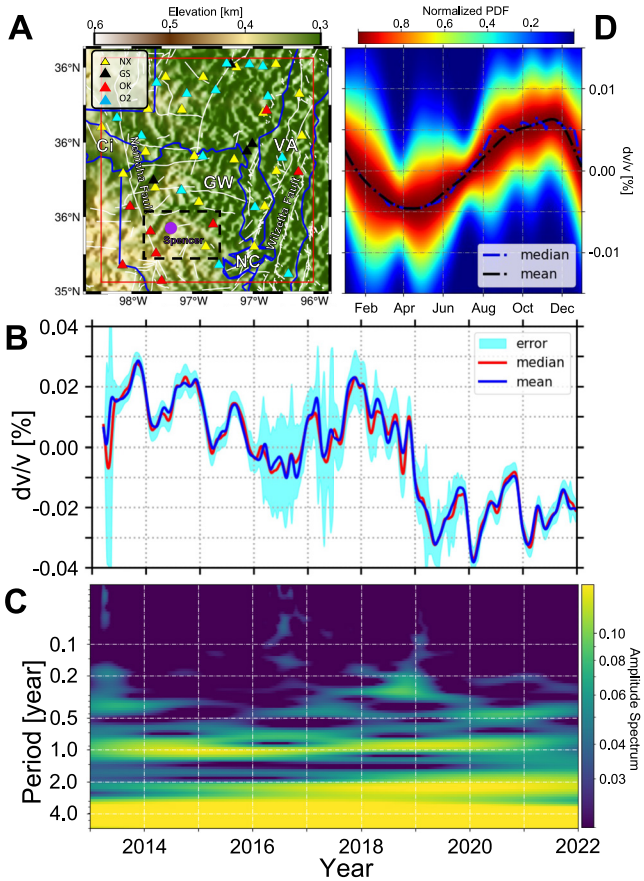

Figure 1. Relative seismic velocity changes measured by ambient noise cross-correlation analysis in central Oklahoma. Available seismometers from different networks are shown as triangles in panel (a). Thin white lines denote fault traces mapped at the Earth's surface (Marsh & Holland, 2016), while thick blue lines represent the boundaries of the Garbar-Wellington aquifer (Garber-Wellington), the Vamoosa-Ada (VA) aquifer (VA), the North Canadian River (NC), and the Cimarron River (Ci) (https://www.owrb.ok.gov/maps). Panel (b) shows the mean (blue) and median (red) values of the estimated velocity variations, while the blue shades represent the standard error of the measurements. The temporal resolution of *dv/v* in panel B is smoothed by a 30-day-long Gaussian filter. Panel (c) illustrates the time frequency analysis of the measured *dv/v* by using short time Fourier analysis. Panel (d) shows the statistical stacking of the annual pattern of *dv/v*.

River (Ci), and North Canadian River (NC) also contribute to the hydrological complexity in the study region (Osborn & Hardy, 1999). In this study, we estimate the seismic velocity variation, *dv/v*, to monitor water storage and drought condition in Oklahoma.

2. Data and Methods

Our study area ranges from 97.90°W to 96.30°W in longitude and 35.20°N to 36.50°N in latitude (Figure 1a). Nine-year-long (from 2013 to 2022) continuous seismic recordings for all available seismometers are collected as the data set for this study. In total, 53 seismometers, from networks NX, OK, GS, and O2, are used in Figure 1a. The spatial and temporal distributions of data availability can be found in Figures S1 and S14 in Supporting Information S1. We set 15 and 100 km as the minimum and maximum for the inter-station distance when grouping station pairs and making time-lapse measurements.

Only vertical components of the broadband seismic recordings are used in the analysis. Due to the imbalanced sampling (data only observed at the Earth's surface) and high susceptibility of shallow structures to failure, large shallow velocity changes can be erroneously mapped to smaller variations at greater depths (Juarez & Ben-Zion, 2020). Here, we estimate the depth sensitivity of our measurements based on fundamental mode Rayleigh waves dispersion with a 1-D velocity profile provided by the OGS (Figure S4 in Supporting Information S1). In order to monitor groundwater storage near the Earth's surface, we filter the continuous recordings from 0.1 to 1.0 Hz, allowing us to map time-lapse velocity changes down to 1.0 km depth. Our data preprocessing procedures include re-sampling, bandpass-filtering, spectral whitening, instrument response deconvolution, and one-bit normalization (Bensen et al., 2007). The continuous recordings, after preprocessing, are cut into one-hour-long segments. For each station pair, the data segments with the same timestamp are cross-correlated and stacked to construct daily cross-correlation functions (CCFs). In order to improve signal-to-noise ratio (SNR), we apply a moving window stacking when computing daily CCFs. When comparing the performance of 60-day-long and 120-day-long stackings (Figure S14 in Supporting Information S1), there is no significant difference in temporal pattern between corresponding *dv/v* curves. For safety, we chose the 60-day-long moving window stacking daily CCFs, which has been used in previous studies (Clements & Denolle, 2018; Lecocq et al., 2017). The reference CCF for each station pair is the stacking of all available daily CCFs, The positive and negative branches of CCF are stacked to further boost SNR. Once we gather the daily and reference CCFs, their relative time shift, *dt*, can be computed by using the Moving Window Cross Spectrum method (MWCS) (Clarke et al., 2011), during which the surface and coda waves are isolated by applying dynamic time windows with apparent velocities of 3.0 and 2.0 km/s, respectively (Figure S5 in Supporting Information S1). With the assumption of a homogeneous and equal-potential stress field, the relative time delay (*dt/t*) between the daily and reference CCFs should be negatively proportional to the velocity variation (*dv/v*), that is, $dv/v = -dt/t$ (Poupinet et al., 1984). In order to remove daily variations and compare with other independent measurements with comparable temporal resolution, the raw *dv/v* is filtered by 7-day-long and 30-day-long Gaussian filters (Figure S6A in Supporting Information S1). The stacking is done on the CCFs, which implies that the derived *dv/v* may not have the same temporal resolution (Figure S7 in Supporting Information S1). More detailed information on the post-processing procedure and analysis of *dv/v* can be found in Section S2 in Supporting Information S1.

We design two additional tests to evaluate the influence of frequency ranges and azimuthal angles on measured *dv/v*. Based on the data set and workflow, four different frequency bands with systematic shift and similar bandwidth (0.1–1.0, 0.3–1.2, 0.5–1.5, and 1.0–2.0 Hz) are used to compute corresponding *dv/v*, which provide similar

seasonal variations and long-term trend in spite of local perturbations (Figure S9 in Supporting Information S1), with an average standard deviation about 0.009%. On the other hand, the CCFs may also be affected by heterogeneous distributions of noise sources, such as periodic ocean tides (Ardhuin et al., 2011; Sens-Schönfelder & Eulenfeld, 2019). Therefore, we group the station pairs and re-calculate *dv/v* according to their azimuthal angles (0°–90°, 90°–180°, 180°–270°, 270–360°) to evaluate the impact of heterogeneous noise source distributions. The similarity among four azimuth groups (Figure S10 in Supporting Information S1), with an averaged standard deviation around 0.013%, suggests that the measured *dv/v* mainly reflect real seismic velocity variations, rather than heterogeneous noise source distributions (Young et al., 1994). These two tests illustrate that the impact of frequency and noise source spatial distribution on *dv/v* measurements are minor. More details about variance estimations can be found in Section S3 in Supporting Information S1.

3. Results

3.1. Seasonal Changes and Long-Term Trends

We compute the mean and median of *dv/v* among all station pairs in order to illustrate the averaged temporal evolution of near-surface seismic velocity in central Oklahoma (Figure 1b). As mentioned, the mean and median values in Figure 1b are smoothed by a 30-day-long Gaussian filter. The raw and smoothed *dv/v* with different Gaussian filters can be found in Figure S6A in Supporting Information S1. The variance of *dv/v* is comparatively small, within 5% for most measurements (blue shade in Figure 1b). Some temporary stations were not working, resulting in relatively larger variance from 2016 to 2018. Since 2014, *dv/v* reduces gradually until the middle of 2017 and then rebounds to its peak value (+0.03%) around the end of 2018 (Figure 1b). After that, it declines further to −0.02% until 2020, and then fluctuates in a relatively low-value zone. Besides this long-term fluctuation, we also observe clear seasonal cycling in *dv/v* measurements. Statistically stacking the intra-annual pattern of each year, we find that *dv/v* declines annually to a trough during the summer time (April to June), whereas its peak value commonly appears in the winter season from October to December (Figure 1d). Both seasonal and long-term changes can be clearly identified by the spectrogram (Figure 1c). A continuous response, centering around 1 year period, reflects the seasonal cycling, while another strong response existing at periods greater than 2 years represents the long-term trend in our measurements.

3.2. Comparison With GRACE Observations

Figure 2 compares the *dv/v* results with the GRACE measurements (Landerer & Swenson, 2012; Richard Peltier et al., 2018; Syed et al., 2008), expressed in terms of water equivalent thickness in centimeters. The gap in the GRACE measurements around 2018 comes from an observational gap between the GRACE and GRACE-FO missions, with the latter launched in May 2018. The sampling rates for both GRACE and GRACE-FO missions are one month. To compare signals, both *dv/v* and GRACE data are interpolated and filtered into the same frequency band. A Gaussian filter with $\sigma = 20$ days is applied to *dv/v* in Figure 2a to focus on long period variations. We further quantify the similarity between GRACE and *dv/v* results by applying a moving window cross-correlation, with a 800-day-long sliding window, between these two time-series (Figure 2b).

Overall, the GRACE data is negatively correlated with our *dv/v* results, and the absolute cross-correlation coefficient in Figure 2b is greater than 0.7 with almost zero time lag, suggesting that gravity perturbations and seismic velocity variations reflect similar environmental changes in central Oklahoma. Furthermore, we use a least-square regression to determine a linear relation between *dv/v* and GRACE results (Δh), which gives $dv/v = -1.68 \times 10^{-3}\Delta h - 9.61 \times 10^{-3}$, with the final data misfit as 0.00848. The confidential ellipse with 2σ (black dashed ellipse in Figure 2c) covers most data points, suggesting a good linear fitting between these two independent datasets. In comparison to the annual statistical stacking of *dv/v* shown in Figure 1d, we also observe seasonal cycling in the GRACE data, but with an opposite intra-annual pattern (Figure 2d). The strong annual similarity between these two independent time series again suggests that they may reflect similar physical processes, such as variations of TWS near the Earth's surface (Famiglietti et al., 2011; Rodell et al., 2007; Tapley, Bettadpur, Ries, et al., 2004). The de-correlation between GRACE measurement and *dv/v* in 2016 might come from the larger variance resulting from the comparatively less sampling. Spatial variation of *dv/v* might be another reason, but we only consider temporal variation in this paper.

As a state-of-the-art tool for monitoring TWS (Rodell et al., 2018), the limited spatial resolution (300–400 km) and temporal sampling (one month) of the GRACE measurements cannot satisfy current requirements of ground

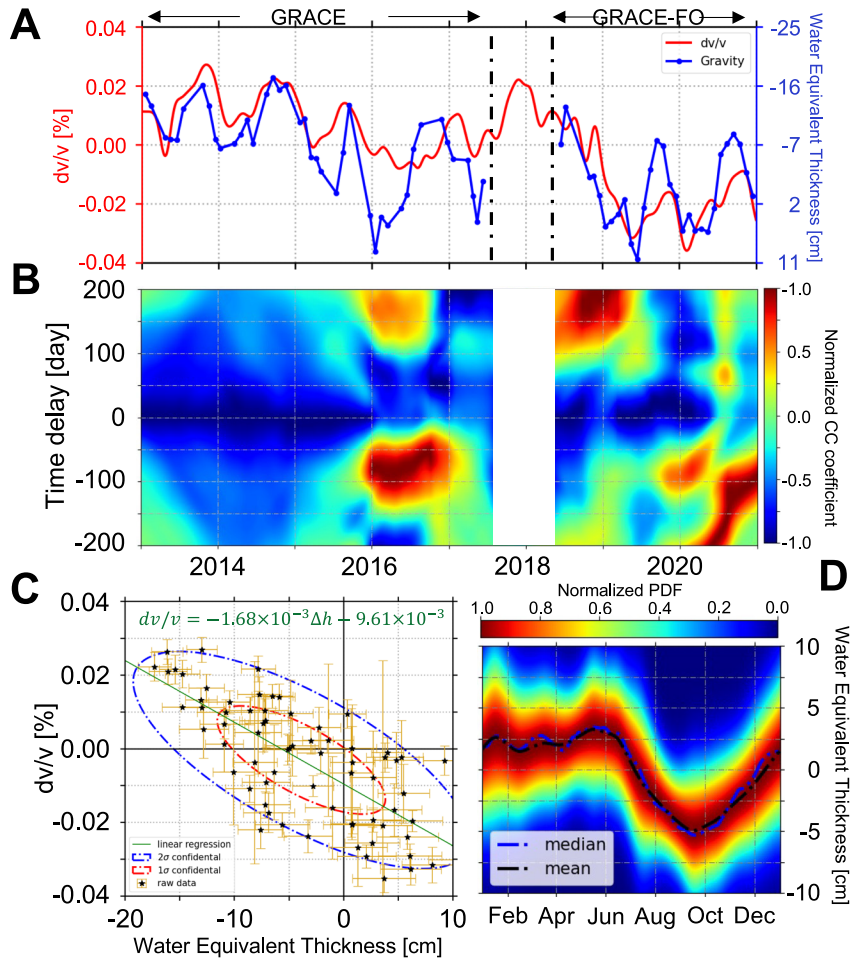

Figure 2. Comparison between relative seismic velocity change (*dv/v*) with Gravity Recovery and Climate Experiment (GRACE) measurements. Panel (a) compares *dv/v* (red) with GRACE measurements (blue) expressed in terms of equivalent water thickness in centimeters. To compare with monthly sampled GRACE measurements, the raw *dv/v* measurement is filtered by a 30-day-long Gaussian filter. Panel (b) illustrates the local cross-correlation map between *dv/v* and GRACE observations. The gap in Panels (a and b) comes from the survey gap between GRACE and GRACE-FO missions. Panel (c) shows the relation between *dv/v* and GRACE results (h) through a linear regression. Yellow bars represent the standard errors of *dv/v* and GRACE measurements. Panel (d) shows the statistical stacking of the annual pattern of the GRACE measurements.

and surface water storage management at regional to local scales. In contrast, seismic ambient noise measurements have the considerably higher temporal and spatial resolution, depending on the specific deployment configuration, and can be used to monitor the intra-seasonal persistence of TWS deficits and surpluses in a relatively small basin with near real-time fashion and low costs. Furthermore, since more than 13,000 permanent seismometers have already been deployed around the world and can be openly accessed through the Data Management Center of the Incorporated Research Institutions for Seismology (IRIS-DMC), continuous seismic noise recordings provide a compelling supplement to the GRACE measurements for monitoring water balance on the Earth's surface.

3.3. Correlation With Groundwater Measurements

As a low-latitude inland state, surface water storage and snowfall are negligible in Oklahoma (Swenson et al., 2008), so groundwater storage and soil moisture are the major contributors to the TWS in Oklahoma. Negative correlations between groundwater levels and *dv/v* have been observed in California (Clements & Denolle, 2018; Mao et al., 2022; Qin et al., 2022) and Germany (Lecocq et al., 2017). Also, the spatiotemporal variations of seismic velocity, after projecting into 2-D maps by using coda wave sensitivity kernels (Mao

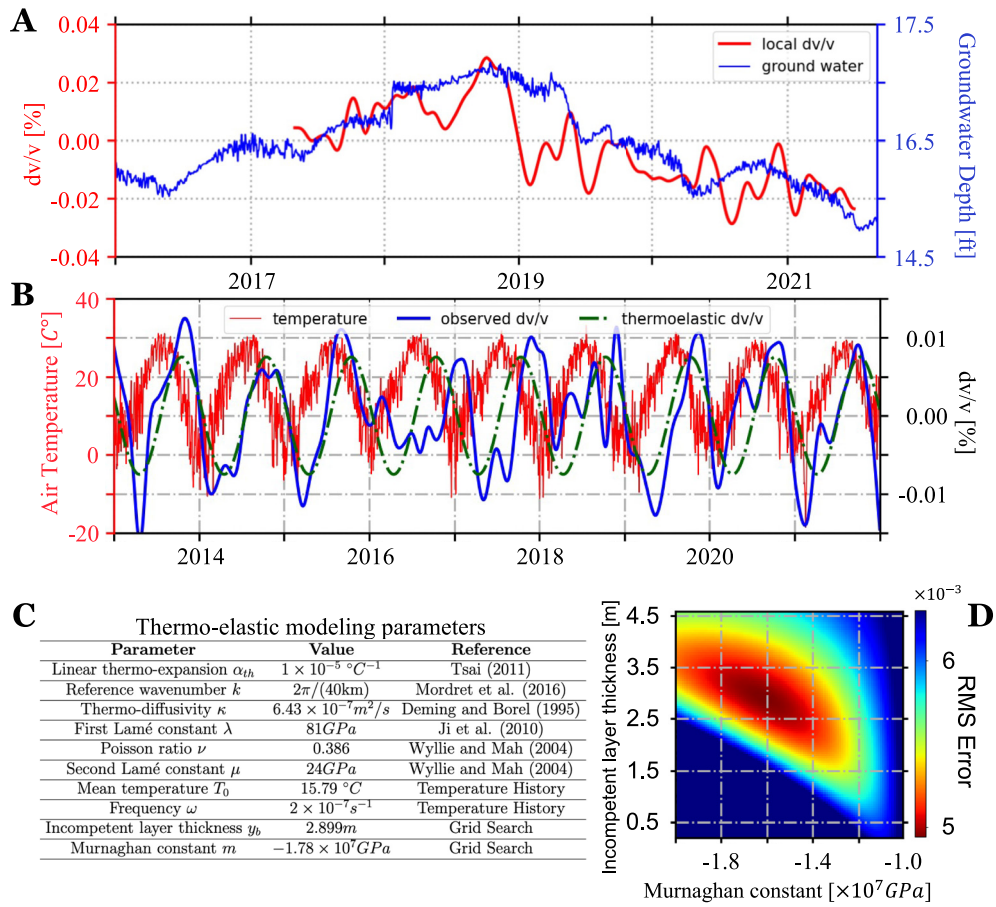

Figure 3. Analysis of potential causes of long-term and seasonal cycling of measured seismic velocity variations. The black line in panel A represents the historical measurement of groundwater depths for the Spencer well (purple dot in Figure 1a), while the red line is the local *dv/v* computed from three seismometers in the vicinity of the well (OK.CHOK, OK.SMO, OK.SWND). The local *dv/v* in panel (a) is smoothed by a 30-day-long filter. Panel (b) compares simulated velocity variations (green dashed line) from a thermo-elastic modeling (Ben-Zion & Leary, 1986; Tsai, 2011) with the historical air temperature (red) recorded in central Oklahoma. Panel (c) gives model parameters used in the thermo-elastic calculation, in which the incompetent layer thickness y_b and the Murnaghan constant m are determined by a grid search shown in panel (d).

et al., 2022), are coherent with the discharge and recharge of aquifers in California. The sensitivity of near-surface seismic velocity to groundwater storage can be directly examined by comparing *dv/v* with groundwater levels.

Deployed by the OGS, the gauge in the Spencer well measures groundwater depths for monitoring the status of the GW aquifer (Mashburn et al., 2018), which can be obtained from the Oklahoma Water Resource Board. Considering lateral variations of seismic velocities, a local *dv/v* is measured from three seismometers (OK.CHOK, OK.SMO, OK.SWND) surrounding the Spencer well (Figure S2 in Supporting Information S1) by using the workflow described in Section 2. The local *dv/v* in Figure 3a is smoothed by a 30-day-long Gaussian filter, although the temporal sampling of the groundwater level in well Spencer is one hour. Starting at 15.5 ft in 2016 (Figure 3a), a monotonic increase of the groundwater depth, indicating a discharge of the GW aquifer, is well correlated with the dynamic increase of seismic velocity around the Spencer well. In contrast, the groundwater level gradually reduces from 17.0 ft in 2019 to 15.0 ft in 2022, representing the recharge of GW aquifer, while the seismic velocity correspondingly decreases by about 0.06% during the same period (Figure 3a). Similar to the gravitational variations shown in Figure 2a, this negative correlation between groundwater levels and long-term trend of local *dv/v* further illustrates the sensitivity of near-surface seismic velocities to groundwater recharge/discharge, and demonstrates the capability of using seismic data to monitor TWS with higher temporal and spatial resolution. The seasonal variations around the long-term changes are modeled in terms of thermo-elastic strain (Figures 3b–3d) and discussed in Section 4.

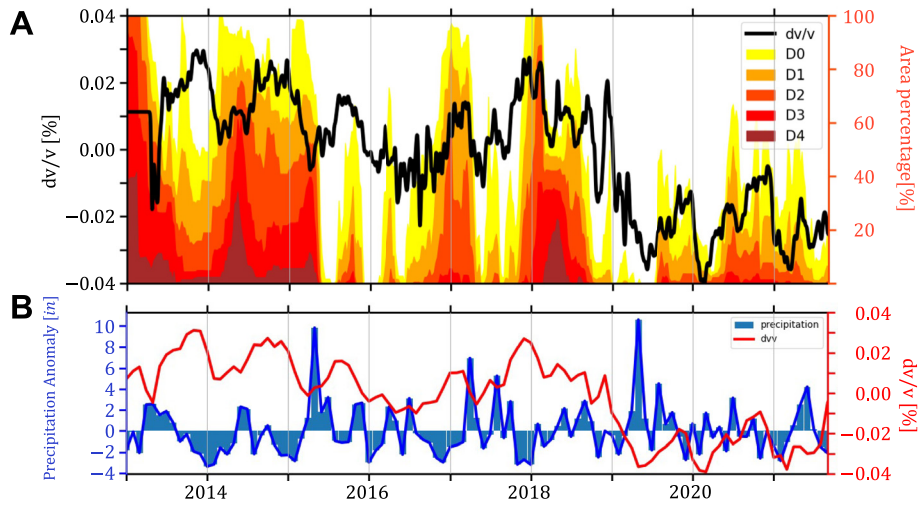

Figure 4. Comparison among *dv/v*, drought index and precipitation records in central Oklahoma. Panel (a) compares measured *dv/v* (black) with drought index from the U.S. Drought Monitor, expressed as the area percentage under different drought categories (droughtmonitor.unl.edu). The severity of drought increases from D0 to D4. Panel (b) presents the monthly precipitation records in central Oklahoma, collected from the Oklahoma Climatological Survey (http://climate.ok.gov). To be comparable with the temporal resolution of drought index (weekly) and precipitation (monthly), *dv/v* is smoothed by 7-day-long and 30-day-long Gaussian filters in panel (a and b), respectively.

3.4. Comparison With Precipitation and Drought Index

Next, we compare the *dv/v* measurements with recordings from precipitation and drought monitoring. Figure 4a shows the history of drought index in central Oklahoma, collected from the USDM (Noel et al., 2020), which classifies the drought condition in five levels, D0 to D4, representing abnormal, moderate, severe, extreme, and exceptional droughts, respectively. From the USDM recordings for central Oklahoma, up to 80% of areas suffered from different levels of drought (D1–D4) from January 2014 to April 2015. Another two severe droughts appeared from November 2016 to May 2017 and December 2017 to October 2018, when 60% of areas in central Oklahoma were under moderate drought (D1) and up to 20% of areas were exceptionally dry (D4).

The drought index is negatively correlated with the precipitation data (Figure 4b) collected from the Oklahoma Climatological Survey (Boone et al., 2012). For instance, no drought is observed in May 2015 and April 2019 when there were high precipitation volumes (greater than +10 inches precipitation anomaly). In contrast, due to comparatively less precipitation in April 2014 (−10 in precipitation anomaly), 40% of areas in central Oklahoma were in D4-level drought. Comparably, the *dv/v* results decrease since February 2014 and reach a minimum in March 2016 when the drought in central Oklahoma is less severe, while they increases during the next severe drought until January 2018 when 90% of areas were in D2-level drought. Because of the frequent and heavy rains in 2019, *dv/v* fluctuates in a relatively low-value zone where only abnormal droughts were detected in central Oklahoma. It is interesting to note that in central Oklahoma, almost every major drought season coincides with a rapid increase of *dv/v*. In order to make a better comparison with monthly recordings of precipitation, we down-sample daily *dv/v* into monthly measurements (Figure 4), We observe that the peaks of precipitation are consistent with the troughs of *dv/v* (such as March 2013, May 2015, and April 2019, etc), while the deficits of precipitation usually occur around the peaks of *dv/v* (October 2015, December 2017, etc). These comparisons among drought index, precipitation, and *dv/v* further support our hypothesis of negative correlation between near-surface seismic velocities and TWS.

4. Discussion

4.1. Potential Impact of Pore Pressure on Seismic Velocity Changes

Seismic velocities within the Earth's uppermost crust may be affected by a variety of factors, including environmental changes (Clements & Denolle, 2018; Hillers et al., 2015; Lecocq et al., 2017; Mao et al., 2022), earthquakes (Bonilla et al., 2019; Brenguier, Campillo, et al., 2008; Peng & Ben-Zion, 2006; Qiu et al., 2020),

and volcanic activities (Brenguier et al., 2014, 2016; Brenguier, Shapiro, et al., 2008; Donaldson et al., 2019; Hotovec-Ellis et al., 2022). Multiple factors can lead to changes in effective confining pressure or dynamic stresses, and eventually result in seismic velocity perturbations with different magnitudes and characteristic time scales. For instance, tides, temperature changes, snow loading, or sea level changes typically produce 10^{-5} to 10^{-3} velocity changes with time scales ranging from hours to years (Taira et al., 2018; Yamamura et al., 2003), whereas tectonic/volcanic activities might also lead to 0.1% to more than 10% velocity perturbations (Brenguier et al., 2014; Niu et al., 2008; Pei et al., 2019). Here, it is important to note that the absolute amplitudes of dv/v depend on the temporal sampling rate (Bonilla et al., 2019), selected lag time (Takano et al., 2019), as well as the loss of sensitivity with respect to the depths (Barajas et al., 2022; Obermann et al., 2013, 2016; Yuan et al., 2021).

Seismic velocity is known to be sensitive to decreasing/increasing effective confining pressure, which affect opening/closure of the microcracks and/or pore space during recharge/discharge of water storage (Birch, 1960; Nur & Simmons, 1969; Simmons, 1964). As we can monitor in-situ seismic velocity variations, a corresponding sensitivity allows estimating changes of effective confining pressure that is relative to water storage in Oklahoma. Here we attempt to calculate the potential stress sensitivity based on the linear regression between dv/v and GRACE measurements (Figure 2c). Since the GRACE measurement is expressed as equivalent water thickness in centimeters (Δh), the slope value connecting gravity and dv/v (-1.68×10^{-3} cm^{-1}) can be transferred to the potential stress sensitivity of dv/v by $\Delta P = \rho g \Delta h$. Converting all variables into standard units, the estimated stress sensitivity is -1.72×10^{-7} Pa^{-1}, which is in the same magnitude as the in situ measurements of previous studies, 10^{-7} Pa^{-1} (Silver et al., 2007; Yamamura et al., 2003). This linear slope also allows estimating, in future studies, the changes of gravity for areas that are too small to be sampled by the GRACE mission. In addition, it provides a possibility to estimate regional stress perturbation from measurements for relative seismic velocity changes.

The clear correlations between our dv/v results with GRACE (Figure 2) and groundwater well measurements (Figure 3a) suggests that when the pore space of sedimentary rocks is filled with water during aquifer recharge, the increasing pore-pressure, and related decreasing effective confining pressure and rock rigidity, generates the reduction of near-surface seismic velocity (Dong & Lu, 2016; Qin et al., 2022). In contrast, the increasing confining pressure and rigidity during drought periods lead to increases in seismic velocity. This helps to explain the correspondence between severe droughts with local peaks in the derived dv/v results shown in Figure 4a.

4.2. Potential Impact of Rock Density Changes on Near-Surface Seismic Velocity

Besides pore pressure changes, bulk density changes may also lead to seismic velocity perturbations. It has been concluded that the bulk density ρ, comparing with shear modulus G, may play a more significant role on shear velocity, with respect to water saturation (Mavko & Jizba, 1991; Nur & Simmons, 1969; M. Wyllie et al., 1962). It has recently been validated in a laboratory experiment (D. Li et al., 2018) that increasing water saturation, from 0 to about 100%, leads to a larger decay in shear velocity than shear modulus solely. We, therefore, discuss the potential impact of density changes on seismic velocity to interpret our results.

To quantitatively investigate the influence of bulk density, we introduce a two-layer conceptual model, with a dry upper layer and a water-saturated lower layer, to represent the aquifer contact. Taking the thicknesses of the dry upper layer and the water table as L_1 and L_2, respectively, the apparent velocity of this two-layer model can be computed by using the following Voigt-Reuss-Hill approximation (Mavko et al., 2020; M. R. J. Wyllie et al., 1956),

$$V_{app} = \frac{L_1}{L_1 + L_2} V_1 + \frac{L_2}{L_1 + L_2} V_2, \tag{1}$$

where V_1 and V_2 stand for the velocities of the upper and lower layers. We assume a homogeneous and isotropic medium in each layer, $V_s = \sqrt{G/\rho}$ (Mavko et al., 2020), and a constant shear modulus G that is unchanged by water saturation for simplicity (Nur & Simmons, 1969; M. Wyllie et al., 1962). With the definition of dry and saturated rocks (Gassmann, 1951), the apparent shear velocity of this two-layer model can be re-written as:

$$\begin{aligned} V_{s,app} &= \frac{L_1}{L_1 + L_2} \sqrt{\frac{G}{\rho_{dry}}} + \frac{L_2}{L_1 + L_2} \sqrt{\frac{G}{\rho_{sat}}}, \\ &= \frac{L_1}{L_1 + L_2} \sqrt{\frac{G}{(1-\phi)\rho_0}} + \frac{L_2}{L_1 + L_2} \sqrt{\frac{G}{(1-\phi)\rho_0 + \phi\rho_w}}. \end{aligned} \tag{2}$$

where ρ_{dry} and ρ_{sat}, controlled by the porosity ϕ, denote the averaged densities of dry and fully saturated rocks, and ρ_0 and ρ_w represent the densities of host rock and pure water, respectively.

To represent the circumstance in Oklahoma, we use $G = 24.0$ GPa, $\phi = 0.3$, and $\rho_0 = 2.65$ g/cm^3 (D. C. Wyllie & Mah, 2004) to approximate the sediment, with $\rho_w = 1.00$ g/cm^3. The total thickness of the two-layer model is $L = L_1 + L_2 = 100$ m, which is equivalent to the average thickness of the GW aquifer (Mashburn et al., 2018). When the groundwater level L_1 changes from 5 to 6 m representing the discharge of the GW aquifer, the apparent shear velocity $V_{s,app}$ reduces by 2.9 m/s with $dv_s/v_s = -0.03\%$, which is comparable to the measured dv/v ($\pm 0.04\%$) from seismic ambient noise recordings (Figure 1b). In spite of the simplification of the model, this synthetic velocity perturbation analysis provides a negative correlation between time-lapse seismic velocity changes and groundwater variations through the change of apparent rock density in water reservoirs.

We provide two possible mechanisms, pore-pressure and bulk density, for interpreting the observed negative correlation between groundwater storage and long-term seismic velocity variations. However, at the current stage, we cannot further distinguish these two mechanisms, or assess the non-uniqueness in modeling and inversion, because of limited knowledge of rock properties in Oklahoma, such as averaged porosity around the water reservoir, elastic moduli of dry rocks, approximated water saturation in dry and wet seasons, confining pressure around aquifers, etc.

4.3. Thermo-Elastic Effects on the Seasonal Changes of Near-Surface Seismic Velocities

Atmospheric temperature variations have been used to explain seasonal and daily changes of dv/v in many regions, including California (Clements & Denolle, 2018, 2023; Hillers et al., 2015; G. Li & Ben-Zion, 2023; Meier et al., 2010; Qiu et al., 2020), Kyushu Island (Q. Wang et al., 2017), northern Chile (Richter et al., 2014), and Mars (Qin et al., 2023). The nonlinear relation between air temperature and seismic velocity changes can be modeled in terms of thermo-elastic strain at the subsurface (Ben-Zion & Leary, 1986; Berger, 1975; Tsai, 2011). This process has been investigated in laboratory experiments by heating and cooling rock samples (Snieder et al., 2002). Here, we use the following expressions of thermo-elastic strain from Ben-Zion and Leary (1986) and Tsai (2011) to explain the relationship between air temperature and seismic velocity in central Oklahoma,

$$\begin{aligned} \frac{\mathrm{d}v}{v} &= A(t)e^{-kz}\frac{\lambda + 3\mu + m}{\mu}\sin(kz)(1-2\nu), \\ A(t) &= \frac{1+\nu}{1-\nu}k\alpha_{th}T_0\sqrt{\frac{\kappa}{\omega}}e^{-\sqrt{\frac{\omega}{2\kappa}}y_b}\cos\left(\omega t - \sqrt{\frac{\omega}{2\kappa}}y_b - \frac{\pi}{4}\right). \end{aligned} \tag{3}$$

Here T_0 and ω denote the mean value and frequency of the temperature record, α_{th} and κ are the linear thermo-expansion coefficient and thermo-diffusivity, respectively, λ and μ are two Lamé parameters, and ν stands for the Poisson's ratio. The values of these model parameters for the study region are collected from previous studies (Deming & Borel, 1995; S. Ji et al., 2010; Zhai et al., 2019), and are listed in Figure 3c. The parameter m in Equation 3 represents the second Murnaghan elastic constant, while y_b represents the thickness of an unconsolidated cover layer. To simulate velocity variations induced by temperature changes, we determine y_b and m by searching for the minimum misfit between observed dv/v and simulated dv/v from Equation 3. This grid-search (Figure 3d) gives values of $y_b = 2.89$ m and $m = -1.78 \times 10^7$ GPa. In reality, most model parameters needed in Equation 3 are spatially varying, however, for simplicity, we use the constant values listed in Figure 3c to represent the entire study area, which lead to regional average estimates of m and y_b.

As shown in Figure 3b, the time series of the simulated (green) and measured (blue) dv/v have good correspondence in both amplitudes and phases with a cross-correlation coefficient of 0.843. The averaged temporal shift between the measured dv/v and temperature fluctuations (red) is around 63 days. The similarity between the simulated and observed seasonal variations of dv/v suggests that air temperature changes are an alternative environmental factor affecting changes of near-surface seismic velocity. A mismatch between the observed and thermo-elastic simulated dv/v is observed from 2016 to 2019, where the time shift ranges from 54 days in 2016 to 12 days in 2019. Similar to the de-correlation between gravity and dv/v in Section 3.2 at almost the same time, this local deviations between simulated and observed dv/v might be related to the large variance in observed dv/v, associated with fewer temporary seismometers from 2016 to 2019. Because of the uncertainty in model parameters, this simulation cannot rigorously delineate the relationship between temperature and seismic velocity, but it provides an alternative explanation about seasonal variations of the seismic velocity.

Furthermore, we use the following linear relation to distinguish the contribution of the thermo-elastic and hydrologic effects,

$$\overline{dv/v} = a \cdot \overline{G} + b \cdot \overline{T} + c, \tag{4}$$

where $\overline{dv/v}$ is the temporal variation of seismic velocity (Figure 1a) after normalization. $\overline{G}$ and $\overline{T}$ represent the normalized gravity and thermo-elastic effects. Equation 4 is solved by least-square regression, which gives $a \approx -0.8$, $b \approx 0.2$ and $c \approx 0.01$ (Figure S11 in Supporting Information S1), suggesting that the hydrologic effect plays a far more important role than the thermo-elastic effect on near-surface velocity changes, which may be due to the frequency bands used in our study.

5. Conclusions

Taking advantage of recently deployed seismometers in central Oklahoma, we estimate relative seismic velocity variations (dv/v) using continuous ambient seismic noise recordings. The negative correlation between dv/v and GRACE measurements, as well as groundwater levels, can be explained by changes of near-surface seismic velocities due to changes of pore pressure and/or bulk density induced by water saturation. The time delay between the seasonal cycling of dv/v and air temperature recordings can be explained in terms of thermo-elastic strain at the subsurface. The simultaneous occurrences of severe droughts and local peaks of dv/v in central Oklahoma illustrate the sensitivity of near-surface seismic velocities to meteorological droughts. Considering the high temporal sampling rates and flexible spatial resolution of seismic recordings, using analyses of the type performed in this paper can improve the ability to monitor terrestrial water distribution, which is critical for sustainable water-resource management and accurate water-deficit estimation.

Data Availability Statement

Seismic recordings for networks NX (https://doi.org/10.7914/SN/NX), GS (https://doi.org/10.7914/SN/OK), O2 (https://doi.org/10.7914/SN/GS) are collected from IRIS-DMC (https://ds.iris.edu/ds/nodes/dmc/). The raw continuous seismic recordings are collected and pre-processed by using Obspy (Beyreuther et al., 2010). The latest version of Obspy (https://doi.org/10.5281/zenodo.6645832) is available in their offical website (https://docs.obspy.org/) and github site (https://github.com/obspy/obspy/). We use MSNoise (https://doi.org/10.5194/tc-2020-267), downloaded from its offical website (https://www.msnoise.org), to measure temporal evolution of near-surface seismic velocity from ambient noise recordings (Lecocq et al., 2014). The groundwater data are collected from the Oklahoma Geological Survey and the Oklahoma Geological Water Resource (https://www.owrb.ok.gov/maps/PMG/owrbdata_GW.html). The historical precipitation recordings for central Oklahoma are accessed from the Oklahoma Climatological Board (https://www.mesonet.org/index.php/weather/monthly_rainfall_table). The historical air temperature recordings in Oklahoma are downloaded from Weather Underground (www.wunderground.com/history). The Colorado Center of Astrodynamics Research compiled the GRACE and GRACE-FO gravitational data (https://ccar.colorado.edu/grace/gsfc.html). The National Drought Mitigation Center at the University of Nebraska-Lincoln provided the historical drought index for central Oklahoma (https://droughtmonitor.unl.edu/DmData/DataDownload/DSCI.aspx).

Acknowledgments
The authors appreciate valuable comments and suggestions from Dr. Marine Denolle and an anonymous referee. This study was supported by the National Science Foundation (Grant EAR-2042098), the U.S. Department of Energy Office of Science (Award DE-SC0016520), and the 3D+4D Seismic Inversion Consortium at the University of Texas at Dallas. We thank the Texas Advanced Computing Center for providing computational facilities for this study. This paper is contribution number 1706 from the Department of Geosciences at the University of Texas at Dallas.

References

Alsdorf, D. E., & Lettenmaier, D. P. (2003). Tracking fresh water from space. *Science*, *301*(5639), 1491–1494. https://doi.org/10.1126/science.1089802

Angerer, E., Crampin, S., Li, X.-Y., & Davis, T. L. (2002). Processing, modelling and predicting time-lapse effects of overpressured fluid-injection in a fractured reservoir. *Geophysical Journal International*, *149*(2), 267–280. https://doi.org/10.1046/j.1365-246X.2002.01607.x

Ardhuin, F., Stutzmann, E., Schimmel, M., & Mangeney, A. (2011). Ocean wave sources of seismic noise. *Journal of Geophysical Research*, *116*(C9), C09004. https://doi.org/10.1029/2011JC006952

Argus, D. F., Heflin, M. B., Peltzer, G., Crampé, F., & Webb, F. H. (2005). Interseismic strain accumulation and anthropogenic motion in metropolitan Los Angeles. *Journal of Geophysical Research*, *110*(B4). https://doi.org/10.1029/2003JB002934

Barajas, A., Margerin, L., & Campillo, M. (2022). Coupled body and surface wave sensitivity kernels for coda-wave interferometry in a three-dimensional scalar scattering medium. *Geophysical Journal International*, *230*(2), 1013–1029. https://doi.org/10.1093/gji/ggac091

Bawden, G. W., Thatcher, W., Stein, R. S., Hudnut, K. W., & Peltzer, G. (2001). Tectonic contraction across Los Angeles after removal of groundwater pumping effects. *Nature*, *412*(6849), 812–815. https://doi.org/10.1038/35090558

Bensen, G., Ritzwoller, M., Barmin, M., Levshin, A. L., Lin, F., Moschetti, M., et al. (2007). Processing seismic ambient noise data to obtain reliable broad-band surface wave dispersion measurements. *Geophysical Journal International*, *169*(3), 1239–1260. https://doi.org/10.1111/j.1365-246X.2007.03374.x

Ben-Zion, Y., & Leary, P. (1986). Thermoelastic strain in a half-space covered by unconsolidated material. *Bulletin of the Seismological Society of America*, *76*(5), 1447–1460. https://doi.org/10.1785/BSSA0760051447

Berger, J. (1975). A note on thermoelastic strains and tilts. *Journal of Geophysical Research*, *80*(2), 274–277. https://doi.org/10.1029/JB080i002p00274

Beyreuther, M., Barsch, R., Krischer, L., Megies, T., Behr, Y., & Wassermann, J. (2010). ObsPy: A Python toolbox for seismology. *Seismological Research Letters*, *81*(3), 530–533. https://doi.org/10.1785/gssrl.81.3.530

Birch, F. (1960). The velocity of compressional waves in rocks to 10 kilobars: 1. *Journal of Geophysical Research*, *65*(4), 1083–1102. https://doi.org/10.1029/JZ065i004p01083

Bonilla, L. F., Guéguen, P., & Ben-Zion, Y. (2019). Monitoring coseismic temporal changes of shallow material during strong ground motion with interferometry and autocorrelation monitoring coseismic temporal changes of shallow material during strong ground motion. *Bulletin of the Seismological Society of America*, *109*(1), 187–198. https://doi.org/10.1785/0120180092

Boone, K. M., McPherson, R. A., Richman, M. B., & Karoly, D. J. (2012). Spatial coherence of rainfall variations using the Oklahoma Mesonet. *International Journal of Climatology*, *32*(6), 843–853. https://doi.org/10.1002/joc.2322

Brenguier, F., Campillo, M., Hadziioannou, C., Shapiro, N. M., Nadeau, R. M., & Larose, É. (2008). Postseismic relaxation along the San Andreas Fault at Parkfield from continuous seismological observations. *Science*, *321*(5895), 1478–1481. https://doi.org/10.1126/science.1160943

Brenguier, F., Campillo, M., Takeda, T., Aoki, Y., Shapiro, N., Briand, X., et al. (2014). Mapping pressurized volcanic fluids from induced crustal seismic velocity drops. *Science*, *345*(6192), 80–82. https://doi.org/10.1126/science.1254073

Brenguier, F., Rivet, D., Obermann, A., Nakata, N., Boué, P., Lecocq, T., et al. (2016). 4-D noise-based seismology at volcanoes: Ongoing efforts and perspectives. *Journal of Volcanology and Geothermal Research*, *321*, 182–195. https://doi.org/10.1016/j.jvolgeores.2016.04.036

Brenguier, F., Shapiro, N. M., Campillo, M., Ferrazzini, V., Duputel, Z., Coutant, O., & Nercessian, A. (2008). Towards forecasting volcanic eruptions using seismic noise. *Nature Geoscience*, *1*(2), 126–130. https://doi.org/10.1038/ngeo104

Campillo, M., & Paul, A. (2003). Long-range correlations in the diffuse seismic coda. *Science*, *299*(5606), 547–549. https://doi.org/10.1126/science.1078551

Claerbout, J. F. (1968). Synthesis of a layered medium from its acoustic transmission response. *Geophysics*, *33*(2), 264–269. https://doi.org/10.1190/1.1439927

Clarke, D., Zaccarelli, L., Shapiro, N., & Brenguier, F. (2011). Assessment of resolution and accuracy of the Moving Window Cross Spectral technique for monitoring crustal temporal variations using ambient seismic noise. *Geophysical Journal International*, *186*(2), 867–882. https://doi.org/10.1111/j.1365-246X.2011.05074.x

Clements, T., & Denolle, M. A. (2018). Tracking groundwater levels using the ambient seismic field. *Geophysical Research Letters*, *45*(13), 6459–6465. https://doi.org/10.1029/2018GL077706

Clements, T., & Denolle, M. A. (2023). The seismic signature of California's earthquakes, droughts, and floods. *Journal of Geophysical Research: Solid Earth*, *128*(1), e2022JB025553. https://doi.org/10.1029/2022JB025553

Deming, D., & Borel, R. A. (1995). Evidence for climatic warming in northcentral Oklahoma from analysis of borehole temperatures. *Journal of Geophysical Research*, *100*(B11), 22017–22032. https://doi.org/10.1029/95JB02625

Donaldson, C., Winder, T., Caudron, C., & White, R. S. (2019). Crustal seismic velocity responds to a magmatic intrusion and seasonal loading in Iceland's Northern Volcanic Zone. *Science Advances*, *5*(11), eaax6642. https://doi.org/10.1126/sciadv.aax6642

Dong, Y., & Lu, N. (2016). Dependencies of shear wave velocity and shear modulus of soil on saturation. *Journal of Engineering Mechanics*, *142*(11), 04016083. https://doi.org/10.1061/(asce)em.1943-7889.0001147

Famiglietti, J. S., Lo, M., Ho, S. L., Bethune, J., Anderson, K., Syed, T. H., et al. (2011). Satellites measure recent rates of groundwater depletion in California's Central Valley. *Geophysical Research Letters*, *38*(3). https://doi.org/10.1029/2010gl046442

Feng, W., Zhong, M., Lemoine, J.-M., Biancale, R., Hsu, H.-T., & Xia, J. (2013). Evaluation of groundwater depletion in North China using the Gravity Recovery and Climate Experiment (GRACE) data and ground-based measurements. *Water Resources Research*, *49*(4), 2110–2118. https://doi.org/10.1002/wrcr.20192

Gassenmeier, M., Sens-Schönfelder, C., Delatre, M., & Korn, M. (2014). Monitoring of environmental influences on seismic velocity at the geological storage site for CO_2 in Ketzin (Germany) with ambient seismic noise. *Geophysical Journal International*, *200*(1), 524–533. https://doi.org/10.1093/gji/ggu413

Gassmann, F. (1951). Elastic waves through a packing of spheres. *Geophysics*, *16*(4), 673–685. https://doi.org/10.1190/1.1437718

Harig, C., & Simons, F. J. (2012). Mapping Greenland's mass loss in space and time. *Proceedings of the National Academy of Sciences*, *109*(49), 19934–19937. https://doi.org/10.1073/pnas.1206785109

Hegarty, S. (2022). Satellites give clues about the coming global harvest. Retrieved from https://www.bbc.com/news/world-62149522

Hillers, G., & Ben-Zion, Y. (2011). Seasonal variations of observed noise amplitudes at 2–18 Hz in southern California. *Geophysical Journal International*, *184*(2), 860–868. https://doi.org/10.1111/j.1365-246X.2010.04886.x

Hillers, G., Ben-Zion, Y., Campillo, M., & Zigone, D. (2015). Seasonal variations of seismic velocities in the San Jacinto fault area observed with ambient seismic noise. *Geophysical Journal International*, *202*(2), 920–932. https://doi.org/10.1093/gji/ggv151

Hotovec-Ellis, A. J., Shiro, B. R., Shelly, D. R., Anderson, K. R., Haney, M. M., Thelen, W. A., et al. (2022). Earthquake-derived seismic velocity changes during the 2018 caldera collapse of Kīlauea volcano. *Journal of Geophysical Research: Solid Earth*, *127*(2), e2021JB023324. https://doi.org/10.1029/2021JB023324

Illien, L., Andermann, C., Sens-Schönfelder, C., Cook, K., Baidya, K., Adhikari, L., & Hovius, N. (2021). Subsurface moisture regulates Himalayan groundwater storage and discharge. *AGU Advances*, *2*(2), e2021AV000398. https://doi.org/10.1029/2021AV000398

James, S., Knox, H., Abbott, R., & Screaton, E. (2017). Improved moving window cross-spectral analysis for resolving large temporal seismic velocity changes in permafrost. *Geophysical Research Letters*, *44*(9), 4018–4026. https://doi.org/10.1002/2016GL072468

Ji, K. H., & Herring, T. A. (2012). Correlation between changes in groundwater levels and surface deformation from GPS measurements in the San Gabriel Valley, California. *Geophysical Research Letters*, *39*(1). https://doi.org/10.1029/2011GL050195

Ji, S., Sun, S., Wang, Q., & Marcotte, D. (2010). Lamé parameters of common rocks in the Earth's crust and upper mantle. *Journal of Geophysical Research*, *115*(B6), B06314. https://doi.org/10.1029/2009JB007134

Juarez, A., & Ben-Zion, Y. (2020). Effects of shallow-velocity reductions on 3D propagation of seismic waves. *Seismological Society of America*, *91*(6), 3313–3322. https://doi.org/10.1785/0220200183

Kamei, R., & Lumley, D. (2017). Full waveform inversion of repeating seismic events to estimate time-lapse velocity changes. *Geophysical Journal International*, *209*(2), 1239–1264. https://doi.org/10.1093/gji/ggx057

Kim, D., & Lekic, V. (2019). Groundwater variations from autocorrelation and receiver functions. *Geophysical Research Letters*, *46*(23), 13722–13729. https://doi.org/10.1029/2019GL084719

Konikow, L. F. (2011). Contribution of global groundwater depletion since 1900 to sea-level rise. *Geophysical Research Letters*, *38*(17). https://doi.org/10.1029/2011GL048604

Kuwayama, Y., Thompson, A., Bernknopf, R., Zaitchik, B., & Vail, P. (2019). Estimating the impact of drought on agriculture using the US Drought Monitor. *American Journal of Agricultural Economics*, *101*(1), 193–210. https://doi.org/10.1093/ajae/aay037

Lanari, R., Lundgren, P., Manzo, M., & Casu, F. (2004). Satellite radar interferometry time series analysis of surface deformation for Los Angeles, California. *Geophysical Research Letters*, *31*(23). https://doi.org/10.1029/2004GL021294

Landerer, F. W., & Swenson, S. (2012). Accuracy of scaled GRACE terrestrial water storage estimates. *Water Resources Research*, *48*(4). https://doi.org/10.1029/2011WR011453

Landrø, M. (2001). Discrimination between pressure and fluid saturation changes from time-lapse seismic data. *Geophysics*, *66*(3), 836–844. https://doi.org/10.1190/1.1444973

Lecocq, T., Caudron, C., & Brenguier, F. (2014). MSNoise, a python package for monitoring seismic velocity changes using ambient seismic noise. *Seismological Research Letters*, *85*(3), 715–726. https://doi.org/10.1785/0220130073

Lecocq, T., Longuevergne, L., Pedersen, H. A., Brenguier, F., & Stammler, K. (2017). Monitoring ground water storage at mesoscale using seismic noise: 30 years of continuous observation and thermo-elastic and hydrological modeling. *Scientific Reports*, *7*(1), 1–16. https://doi.org/10.1785/0220130073

Li, D., Wei, J., Di, B., Ding, P., Huang, S., & Shuai, D. (2018). Experimental study and theoretical interpretation of saturation effect on ultrasonic velocity in tight sandstones under different pressure conditions. *Geophysical Journal International*, *212*(3), 2226–2237. https://doi.org/10.1093/gji/ggx536

Li, G., & Ben-Zion, Y. (2023). Daily and seasonal variations of shallow seismic velocities in southern California from joint analysis of H/V ratios and autocorrelations of seismic waveforms. *Journal of Geophysical Research: Solid Earth*, *128*(2), e2022JB025682. https://doi.org/10.1029/2022JB025682

Lin, F.-C., Moschetti, M. P., & Ritzwoller, M. H. (2008). Surface wave tomography of the western United States from ambient seismic noise: Rayleigh and Love wave phase velocity maps. *Geophysical Journal International*, *173*(1), 281–298. https://doi.org/10.1111/j.1365-246X.2008.03720.x

Lindner, F., Wassermann, J., & Igel, H. (2021). Seasonal freeze-thaw cycles and permafrost degradation on Mt. Zugspitze (German/Austrian Alps) revealed by single-station seismic monitoring. *Geophysical Research Letters*, *48*(18), e2021GL094659. https://doi.org/10.1029/2021GL094659

Liu, Z., Huang, J., Peng, Z., & Su, J. (2014). Seismic velocity changes in the epicentral region of the 2008 Wenchuan earthquake measured from three-component ambient noise correlation techniques. *Geophysical Research Letters*, *41*(1), 37–42. https://doi.org/10.1002/2013GL058682

Lobkis, O. I., & Weaver, R. L. (2001). On the emergence of the Green's function in the correlations of a diffuse field. *Journal of the Acoustical Society of America*, *110*(6), 3011–3017. https://doi.org/10.1785/0220190053

Long, D., Scanlon, B. R., Longuevergne, L., Sun, A. Y., Fernando, D. N., & Save, H. (2013). GRACE satellite monitoring of large depletion in water storage in response to the 2011 drought in Texas. *Geophysical Research Letters*, *40*(13), 3395–3401. https://doi.org/10.1002/grl.50655

Lu, Y., & Ben-Zion, Y. (2022). Regional seismic velocity changes following the 2019 M w 7.1 Ridgecrest, California earthquake from autocorrelations and P/S converted waves. *Geophysical Journal International*, *228*(1), 620–630. https://doi.org/10.1093/gji/ggab350

Lumley, D. (2010). 4D seismic monitoring of CO 2 sequestration. *The Leading Edge*, *29*(2), 150–155. https://doi.org/10.1190/1.3304817

Lumley, D. E. (2001). Time-lapse seismic reservoir monitoring. *Geophysics*, *66*(1), 50–53. https://doi.org/10.1190/1.1444921

Mao, S., Campillo, M., van Der Hilst, R. D., Brenguier, F., Stehly, L., & Hillers, G. (2019). High temporal resolution monitoring of small variations in crustal strain by dense seismic arrays. *Geophysical Research Letters*, *46*(1), 128–137. https://doi.org/10.1029/2018GL079944

Mao, S., Lecointre, A., van der Hilst, R. D., & Campillo, M. (2022). Space-time monitoring of groundwater fluctuations with passive seismic interferometry. *Nature Communications*, *13*(1), 1–9. https://doi.org/10.1038/s41467-022-32194-3

Marsh, S., & Holland, A. (2016). Comprehensive fault database and interpretive fault map of Oklahoma (Tech. Rep.). Oklahoma Geological Survey. Retrieved from http://ogs.ou.edu/docs/openfile/OF2-2016.pdf

Mashburn, S. L., Ryter, D., Neel, C. R., Smith, S. J., & Magers, J. S. (2018). Hydrogeology and simulation of groundwater flow in the Central Oklahoma (Garber-Wellington) Aquifer, Oklahoma, 1987 to 2009, and simulation of available water in storage (pp. 2010–2059). https://doi.org/10.3133/sir20135219

Mavko, G., & Jizba, D. (1991). Estimating grain-scale fluid effects on velocity dispersion in rocks. *Geophysics*, *56*(12), 1940–1949. https://doi.org/10.1190/1.1443005

Mavko, G., Mukerji, T., & Dvorkin, J. (2020). *The rock physics handbook*. Cambridge university press. https://doi.org/10.1017/CBO9780511626753

Meier, U., Shapiro, N. M., & Brenguier, F. (2010). Detecting seasonal variations in seismic velocities within Los Angeles basin from correlations of ambient seismic noise. *Geophysical Journal International*, *181*(2), 985–996. https://doi.org/10.1111/j.1365-246X.2010.04550.x

Minato, S., Tsuji, T., Ohmi, S., & Matsuoka, T. (2012). Monitoring seismic velocity change caused by the 2011 Tohoku-oki earthquake using ambient noise records. *Geophysical Research Letters*, *39*(9). https://doi.org/10.1029/2012GL051405

Nakata, R., Jang, U.-G., Lumley, D., Mouri, T., Nakatsukasa, M., Takanashi, M., & Kato, A. (2022). Seismic time-lapse monitoring of near-surface microbubble water injection by full waveform inversion. *Geophysical Research Letters*, *49*(24), e2022GL098734. https://doi.org/10.1029/2022GL098734

Niu, F., Silver, P. G., Daley, T. M., Cheng, X., & Majer, E. L. (2008). Preseismic velocity changes observed from active source monitoring at the Parkfield SAFOD drill site. *Nature*, *454*(7201), 204–208. https://doi.org/10.1038/nature07111

Noel, M., Bathke, D., Fuchs, B., Gutzmer, D., Haigh, T., Hayes, M., et al. (2020). Linking drought impacts to drought severity at the state level. *Bulletin of the American Meteorological Society*, *101*(8), E1312–E1321. https://doi.org/10.1175/BAMS-D-19-0067.1

Nur, A., & Simmons, G. (1969). The effect of saturation on velocity in low porosity rocks. *Earth and Planetary Science Letters*, *7*(2), 183–193. https://doi.org/10.1016/0012-821X(69)90035-1

Obermann, A., Planes, T., Hadziioannou, C., & Campillo, M. (2016). Lapse-time-dependent coda-wave depth sensitivity to local velocity perturbations in 3-D heterogeneous elastic media. *Geophysical Journal International*, *207*(1), 59–66. https://doi.org/10.1093/gji/ggw264

Obermann, A., Planès, T., Larose, E., Sens-Schönfelder, C., & Campillo, M. (2013). Depth sensitivity of seismic coda waves to velocity perturbations in an elastic heterogeneous medium. *Geophysical Journal International*, *194*(1), 372–382. https://doi.org/10.1093/gji/ggt043

Oki, T., & Kanae, S. (2006). Global hydrological cycles and world water resources. *Science*, *313*(5790), 1068–1072. https://doi.org/10.1126/science.1128845

Osborn, N. I., & Hardy, R. H. (1999). *Statewide groundwater vulnerability map of Oklahoma (tech. Rep.)*. Oklahoma Water Resources Board Oklahoma City. Retrieved from https://www.owrb.ok.gov/studies/reports/gwvulnerability/entire-report.pdf

Pei, S., Niu, F., Ben-Zion, Y., Sun, Q., Liu, Y., Xue, X., et al. (2019). Seismic velocity reduction and accelerated recovery due to earthquakes on the Longmenshan fault. *Nature Geoscience*, *12*(5), 387–392. https://doi.org/10.1038/s41561-019-0347-1

Peng, Z., & Ben-Zion, Y. (2006). Temporal changes of shallow seismic velocity around the Karadere-Düzce branch of the north Anatolian fault and strong ground motion. *Pure and Applied Geophysics*, *163*(2–3), 567–600. https://doi.org/10.1007/s00024-005-0034-6

Pokhrel, Y., Felfelani, F., Satoh, Y., Boulange, J., Burek, P., Gädeke, A., et al. (2021). Global terrestrial water storage and drought severity under climate change. *Nature Climate Change*, *11*(3), 226–233. https://doi.org/10.1038/s41558-020-00972-w

Poupinet, G., Ellsworth, W., & Frechet, J. (1984). Monitoring velocity variations in the crust using earthquake doublets: An application to the Calaveras Fault, California. *Journal of Geophysical Research*, *89*(B7), 5719–5731. https://doi.org/10.1029/JB089iB07p05719

Qin, L., Qiu, H., Nakata, N., Deng, S., Levander, A., & Ben-Zion, Y. (2023). Variable daily autocorrelation functions of high-frequency seismic data on Mars. *Seismological Research Letters*, *12*(2A), 746–758. https://doi.org/10.1785/0220220196

Qin, L., Steidl, J. H., Qiu, H., Nakata, N., & Ben-Zion, Y. (2022). Monitoring seasonal shear wave velocity changes in the top 6 m at Garner Valley in Southern California with borehole data. *Geophysical Research Letters*, *49*(23), e2022GL101189. https://doi.org/10.1029/2022GL101189

Qiu, H., Hillers, G., & Ben-Zion, Y. (2020). Temporal changes of seismic velocities in the San Jacinto Fault zone associated with the 2016 Mw 5.2 Borrego Springs earthquake. *Geophysical Journal International*, *220*(3), 1536–1554. https://doi.org/10.1093/gji/ggz538

Reager, J., Gardner, A., Famiglietti, J., Wiese, D., Eicker, A., & Lo, M.-H. (2016). A decade of sea level rise slowed by climate-driven hydrology. *Science*, *351*(6274), 699–703. https://doi.org/10.1126/science.aad8386

Reager, J. T., Thomas, B. F., & Famiglietti, J. S. (2014). River basin flood potential inferred using GRACE gravity observations at several months lead time. *Nature Geoscience*, *7*(8), 588–592. https://doi.org/10.1038/ngeo2203

Richard Peltier, W., Argus, D. F., & Drummond, R. (2018). Comment on "An assessment of the ICE-6G_C (VM5a) glacial isostatic adjustment model" by Purcell et al. *Journal of Geophysical Research: Solid Earth*, *123*(2), 2019–2028. https://doi.org/10.1002/2016JB013844

Richter, T., Sens-Schönfelder, C., Kind, R., & Asch, G. (2014). Comprehensive observation and modeling of earthquake and temperature-related seismic velocity changes in northern Chile with passive image interferometry. *Journal of Geophysical Research: Solid Earth*, *119*(6), 4747–4765. https://doi.org/10.1002/2013JB010695

Rickett, J., & Lumley, D. (2001). Cross-equalization data processing for time-lapse seismic reservoir monitoring: A case study from the Gulf of Mexico. *Geophysics*, *66*(4), 1015–1025. https://doi.org/10.1190/1.1487049

Ritzwoller, M. H., Lin, F.-C., & Shen, W. (2011). Ambient noise tomography with a large seismic array. *Comptes Rendus Geoscience*, *343*(8–9), 558–570. https://doi.org/10.1016/j.crte.2011.03.007

Rodell, M., Chen, J., Kato, H., Famiglietti, J. S., Nigro, J., & Wilson, C. R. (2007). Estimating groundwater storage changes in the Mississippi River basin (USA) using GRACE. *Hydrogeology Journal*, *15*(1), 159–166. https://doi.org/10.1007/s10040-006-0103-7

Rodell, M., Famiglietti, J. S., Wiese, D. N., Reager, J., Beaudoing, H. K., Landerer, F. W., & Lo, M.-H. (2018). Emerging trends in global freshwater availability. *Nature*, *557*(7707), 651–659. https://doi.org/10.1038/s41586-018-0123-1

Rodell, M., Velicogna, I., & Famiglietti, J. S. (2009). Satellite-based estimates of groundwater depletion in India. *Nature*, *460*(7258), 999–1002. https://doi.org/10.1038/nature08238

Rubinstein, J. L., Uchida, N., & Beroza, G. C. (2007). Seismic velocity reductions caused by the 2003 Tokachi-Oki earthquake. *Journal of Geophysical Research*, *112*(B5), B05315. https://doi.org/10.1029/2006JB004440

Scanlon, B. R., Faunt, C. C., Longuevergne, L., Reedy, R. C., Alley, W. M., McGuire, V. L., & McMahon, P. B. (2012). Groundwater depletion and sustainability of irrigation in the US High Plains and Central Valley. *Proceedings of the National Academy of Sciences*, *109*(24), 9320–9325. https://doi.org/10.1073/pnas.1200311109

Sens-Schönfelder, C., & Eulenfeld, T. (2019). Probing the in situ elastic nonlinearity of rocks with earth tides and seismic noise. *Physical Review Letters*, *122*(13), 138501. https://doi.org/10.1103/PhysRevLett.122.138501

Sens-Schönfelder, C., & Wegler, U. (2006). Passive image interferometry and seasonal variations of seismic velocities at Merapi Volcano, Indonesia. *Geophysical Research Letters*, *33*(21), L21302. https://doi.org/10.1029/2006GL027797

Shapiro, N. M., Campillo, M., Stehly, L., & Ritzwoller, M. H. (2005). High-resolution surface-wave tomography from ambient seismic noise. *Science*, *307*(5715), 1615–1618. https://doi.org/10.1126/science.1108339

Silver, P. G., Daley, T. M., Niu, F., & Majer, E. L. (2007). Active source monitoring of cross-well seismic travel time for stress-induced changes. *Bulletin of the Seismological Society of America*, *97*(1B), 281–293. https://doi.org/10.1785/0120060120

Simmons, G. (1964). Velocity of shear waves in rocks to 10 kilobars, 1. *Journal of Geophysical Research*, *69*(6), 1123–1130. https://doi.org/10.1029/JZ069i006p01123

Snieder, R. (2006). The theory of coda wave interferometry. *Pure and Applied Geophysics*, *163*(2–3), 455–473. https://doi.org/10.1007/s00024-005-0026-6

Snieder, R., Grêt, A., Douma, H., & Scales, J. (2002). Coda wave interferometry for estimating nonlinear behavior in seismic velocity. *Science*, *295*(5563), 2253–2255. https://doi.org/10.1126/science.1070015

Svoboda, M., LeComte, D., Hayes, M., Heim, R., Gleason, K., Angel, J., et al. (2002). The drought monitor. *Bulletin of the American Meteorological Society*, *83*(8), 1181–1190. https://doi.org/10.1175/1520-0477-83.8.1181

Swenson, S., Famiglietti, J., Basara, J., & Wahr, J. (2008). Estimating profile soil moisture and groundwater variations using GRACE and Oklahoma Mesonet soil moisture data. *Water Resources Research*, *44*(1). https://doi.org/10.1029/2007WR006057

Syed, T. H., Famiglietti, J. S., Rodell, M., Chen, J., & Wilson, C. R. (2008). Analysis of terrestrial water storage changes from GRACE and GLDAS. *Water Resources Research*, *44*(2). https://doi.org/10.1029/2006WR005779

Taira, T., Brenguier, F., & Kong, Q. (2015). Ambient noise-based monitoring of seismic velocity changes associated with the 2014 Mw 6.0 South Napa earthquake. *Geophysical Research Letters*, *42*(17), 6997–7004. https://doi.org/10.1002/2015GL065308

Taira, T., Nayak, A., Brenguier, F., & Manga, M. (2018). Monitoring reservoir response to earthquakes and fluid extraction, Salton Sea geothermal field, California. *Science Advances*, *4*(1), e1701536. https://doi.org/10.1126/sciadv.1701536

Takano, T., Nishimura, T., Nakahara, H., Ueda, H., & Fujita, E. (2019). Sensitivity of seismic velocity changes to the tidal strain at different lapse times: Data analyses of a small seismic array at Izu-Oshima volcano. *Journal of Geophysical Research: Solid Earth*, *124*(3), 3011–3023. https://doi.org/10.1029/2018JB016235

Tapley, B. D., Bettadpur, S., Ries, J. C., Thompson, P. F., & Watkins, M. M. (2004). GRACE measurements of mass variability in the Earth system. *Science*, *305*(5683), 503–505. https://doi.org/10.1126/science.1099192

Tapley, B. D., Bettadpur, S., Watkins, M., & Reigber, C. (2004). The gravity recovery and climate experiment: Mission overview and early results. *Geophysical Research Letters*, *31*(9). https://doi.org/10.1029/2004GL019920

Tian, S., Tregoning, P., Renzullo, L. J., van Dijk, A. I., Walker, J. P., Pauwels, V. R., & Allgeyer, S. (2017). Improved water balance component estimates through joint assimilation of GRACE water storage and SMOS soil moisture retrievals. *Water Resources Research*, *53*(3), 1820–1840. https://doi.org/10.1002/2016WR019641

Tsai, V. C. (2011). A model for seasonal changes in GPS positions and seismic wave speeds due to thermoelastic and hydrologic variations. *Journal of Geophysical Research*, *116*(B4), B04404. https://doi.org/10.1029/2010JB008156

Velicogna, I., & Wahr, J. (2006a). Acceleration of Greenland ice mass loss in spring 2004. *Nature*, *443*(7109), 329–331. https://doi.org/10.1038/nature05168

Velicogna, I., & Wahr, J. (2006b). Measurements of time-variable gravity show mass loss in Antarctica. *Science*, *311*(5768), 1754–1756. https://doi.org/10.1126/science.1123785

Wang, H. F. (2017). *Theory of linear poroelasticity with applications to geomechanics and hydrogeology*. Princeton University Press.

Wang, Q., Brenguier, F., Campillo, M., Lecointre, A., Takeda, T., & Aoki, Y. (2017). Seasonal crustal seismic velocity changes throughout Japan. *Journal of Geophysical Research: Solid Earth*, *122*(10), 7987–8002. https://doi.org/10.1002/2017JB014307

Wapenaar, K., & Fokkema, J. (2006). Green's function representations for seismic interferometry. *Geophysics*, *71*(4), SI33–SI46. https://doi.org/10.1190/1.2213955

Watson, K. M., Bock, Y., & Sandwell, D. T. (2002). Satellite interferometric observations of displacements associated with seasonal groundwater in the Los Angeles basin. *Journal of Geophysical Research*, *107*(B4), ETG8-1–ETG8-15. https://doi.org/10.1029/2001JB000470

Wu, W., Zhan, Z., Peng, S., Ni, S., & Callies, J. (2020). Seismic ocean thermometry. *Science*, *369*(6510), 1510–1515. https://doi.org/10.1126/science.abb9519

Wyllie, D. C., & Mah, C. (2004). *Rock slope engineering*. CRC Press.

Wyllie, M., Gardner, G., & Gregory, A. (1962). Studies of elastic wave attenuation in porous media. *Geophysics*, *27*(5), 569–589. https://doi.org/10.1190/1.1439063

Wyllie, M. R. J., Gregory, A. R., & Gardner, L. W. (1956). Elastic wave velocities in heterogeneous and porous media. *Geophysics*, *21*(1), 41–70. https://doi.org/10.1190/1.1438217

Yamamura, K., Sano, O., Utada, H., Takei, Y., Nakao, S., & Fukao, Y. (2003). Long-term observation of in situ seismic velocity and attenuation. *Journal of Geophysical Research*, *108*(B6). https://doi.org/10.1029/2002JB002005

Yao, H., & Van Der Hilst, R. D. (2009). Analysis of ambient noise energy distribution and phase velocity bias in ambient noise tomography, with application to SE Tibet. *Geophysical Journal International*, *179*(2), 1113–1132. https://doi.org/10.1111/j.1365-246X.2009.04329.x

Young, C. J., Chael, E. P., Zagar, D. A., & Carter, J. A. (1994). Variations in noise and signal levels in a pair of deep boreholes near Amarillo, Texas. *Bulletin of the Seismological Society of America*, *84*(5), 1593–1607. https://doi.org/10.1785/BSSA0840051593

Yuan, C., Bryan, J., & Denolle, M. (2021). Numerical comparison of time-frequency-and wavelet-domain methods for coda wave interferometry. *Geophysical Journal International*, *226*(2), 828–846. https://doi.org/10.1093/gji/ggab140

Zhai, G., Shirzaei, M., Manga, M., & Chen, X. (2019). Pore-pressure diffusion, enhanced by poroelastic stresses, controls induced seismicity in Oklahoma. *Proceedings of the National Academy of Sciences*, *116*(33), 16228–16233. https://doi.org/10.1073/pnas.1819225116

Zhu, T., Ajo-Franklin, J., Daley, T. M., & Marone, C. (2019). Dynamics of geologic CO2 storage and plume motion revealed by seismic coda waves. *Proceedings of the National Academy of Sciences*, *116*(7), 2464–2469. https://doi.org/10.1073/pnas.1810903116